

pubs.acs.org/cm Article

Using Redox Titrations to Probe the Role of Trivalent Impurity Ions in the Ferromagnetism of Colloidal EuS Nanocrystals

Michael C. De Siena, Alexander G. Rachkov, Rachel Fainblat, Derak James, Sidney E. Creutz, Sarah L. Stoll,* and Daniel R. Gamelin*



Cite This: Chem. Mater. 2020, 32, 8633-8640



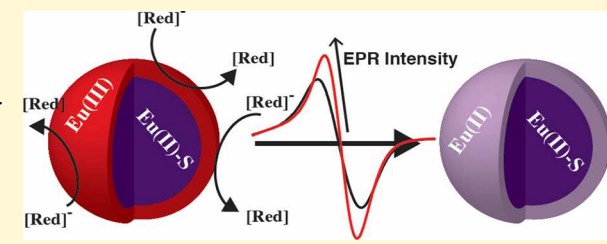
ACCESS

Metrics & More

Article Recommendations

Supporting Information

ABSTRACT: EuS and related ferromagnetic semiconductors have long been model materials for spintronic device functionality because of their ability to generate highly spin-polarized electrical currents. Although the low Curie temperature ($T_{\rm C}$) of EuS limits practical implementation of such devices, the $T_{\rm C}$ of bulk EuS can be raised by n-doping with trivalent impurity ions such as ${\rm Gd}^{3+}$. Such doping introduces free conduction-band electrons that strengthen the magnetic exchange, raising $T_{\rm C}$. In EuS nanostructures, analogous doping has also been explored. Paradoxically, such nanostructures also have a tendency to



show native Eu³⁺ "impurities". It is unclear what impact these impurities or non-native trivalent impurities may have on magnetic ordering. Here, we report spectroscopic, magnetic, and redox-chemical studies aimed at assessing the role of trivalent impurities in the ferromagnetism of colloidal EuS nanocrystals. Combining postsynthetic redox chemistry with optical and electron paramagnetic resonance (EPR) spectroscopic measurements, we show that reduction of native Eu³⁺ impurities to Eu²⁺ increases the overall magnetization below $T_{\rm C}$ and simultaneously decreases $T_{\rm C}$ by \sim 7%, with no evidence of free conduction-band electrons at any stage. The data suggest that some of the newly formed Eu²⁺ ions participate in the ferromagnetic ordering despite having a different coordination environment than the Eu²⁺ ions of the as-synthesized nanocrystals (e.g., surface vs core Eu²⁺), and we hypothesize that surface-localized charge compensation and the very negative EuS conduction-band-edge potential prevent n-doping in these nanocrystals. These results demonstrate postsynthetic chemical modulation of the ferromagnetism of colloidal EuS nanocrystals and additionally provide a well-controlled assessment of the contribution of trivalent impurity ions to this magnetism.

■ INTRODUCTION

Europium(II) monochalcogenides are a classic group of magnetic semiconductors, displaying rich magnetic ordering ranging from ferromagnetism for EuO and EuS to metamagnetism for EuSe and antiferromagnetism for EuTe. EuS in particular displays a high degree of electron-spin polarization in transport measurements, making this material a model system for exploration of spintronic technologies such as spin filters and spin valves. $^{2-4}$ The low Curie temperature of EuS ($T_{\rm C}$ = 16.6 K)¹ limits its practical use, but aliovalent doping, typically with Gd^{3+} (also S = 7/2), has been shown to increase T_C in both bulk¹ and nanocrystalline EuS. 1,5,6 Aliovalent doping generates delocalized conduction-band (CB) electrons that enhance the indirect interlanthanide exchange coupling, thereby stabilizing ferromagnetic ordering. 1,5-7 The correlation between free carriers and T_C in Eu_{1-x}Gd_xO films grown by MBE was demonstrated by resistivity measurements,8 and spectroscopic signatures of free carriers by mid-infrared (mid-IR) intra-CB absorption ^{1,9-13} and a temperature-dependent red-shift of the interband absorption edge ^{10,11} have provided independent support for this mechanism. $T_{\rm C}$ enhancement has additionally been observed for doping with nonmagnetic trivalent lanthanides such as ${\rm La}^{3+}$ or ${\rm Lu}^{3+}$ in EuO, but these

ions appear to also cause magnetic disorder. ¹⁴ The magnetism becomes more complicated when the dopant is redox active, such as $\rm Sm^{3+/2+}$. In bulk Sm-doped EuO, Sm is trivalent, introducing free electrons and increasing $T_{\rm C}$. ¹⁵ In bulk Sm-doped EuS, however, Sm is divalent and only *decreases* the overall magnetization through spin dilution. ¹⁶ By changing the lattice anion, therefore, the Sm oxidation state is changed and its influence on the material's magnetic properties is different. This comparison suggests the intriguing possibility that redox transformations of europium itself (for which both $\rm Eu^{2+}$ and $\rm Eu^{3+}$ are often readily accessible) may possibly influence the magnetic and optical properties of nominally *undoped* europium chalcogenides, providing a new entry into tunable magneto-electronic properties in this class of magnetic materials.

Received: July 21, 2020 Revised: September 10, 2020 Published: September 14, 2020





Colloidal EuS nanostructures have been explored as promising solution-processable low-dimensional magnetic semiconductors that can be interfaced with other materials and whose magnetic properties can potentially be tuned by controlling nanocrystallite size, shape, and surface chemistry. 17-23 The high surface-to-volume ratios of such nanostructures present complications in terms of stability, crystallinity, and the general difficulty of controlling the speciation of surface ions and ligands. In particular, as-synthesized EuS nanocrystals (NCs) frequently show partial oxidation of Eu²⁺ to Eu^{3+,20,22} generally assumed to occur predominantly in amorphous surface layers. 18,24,25 To the extent that such Eu³⁺ ions can be considered as aliovalent impurities, they should behave similarly to the Gd³⁺, Sm³⁺, or other trivalent dopants described above. Although the presence of such Eu³⁺ is widely recognized, their effect on the magnetism of EuS nanostructures has not yet been addressed.

The research reported here aims to answer two main questions—first, do Eu³⁺ impurities in EuS NCs introduce free charge carriers, as observed with other trivalent dopants in bulk EuS? Second, can the oxidation state of these Eu³⁺ ions be controlled postsynthetically, thereby modulating the magnetic properties of the NCs? To address these questions, we used chemical reductants to tune the Eu³⁺/Eu²⁺ ratios in colloidal EuS NCs, and we characterized the resulting NCs using optical and electron paramagnetic resonance (EPR) spectroscopies. We show that the Eu3+ impurities in as-synthesized NCs are not charge-compensated by excess CB electrons, and we hypothesize that their excess positive charges are instead compensated by localized surface counter-charges. Additionally, we demonstrate for the first time that it is possible to reduce these native Eu³⁺ ions to Eu²⁺ in free-standing colloidal EuS NCs. This reduction does indeed have a modest but clearly detectable impact on the NC magnetism, reducing T_C by $\sim 7\%$ (from 16.1 to 15.0 K) and increasing the magnetization below T_C . Spectroscopic and magnetic evidence suggests that the newly formed Eu2+ ions also order ferromagnetically, in part, but also that they have a slightly different coordination environment than the Eu²⁺ ions present in the as-synthesized NCs, possibly due to surface proximity.

■ EXPERIMENTAL METHODS

General Considerations. Unless otherwise stated, all measurements and synthetic manipulations were performed using standard Schlenk techniques under a dinitrogen atmosphere or in a glovebox under an atmosphere of purified dinitrogen. Anhydrous tetrahydrofuran (THF) was purified through an alumina column pressurized with Ar.

Chemicals. Unless otherwise stated, all chemicals were used as purchased without further purification. Anthracene (99%), decamethylcobaltocene (CoCp*₂), mercury (≥99.99%), naphthalene (99%), 1-octadecene (ODE, 90%), oleylamine (OLA, 70%), and trioctylphosphine (TOP, >97%) were purchased from Sigma-Aldrich. 2-Methyltetrahydrofuran (2-MeTHF, anhydrous, ≥99.0%, Sigma-Aldrich) was further dried over sodium benzophenone and distilled before use. Diethylammonium diethyldithiocarbamate ((NH₂Et₂)-(S₂CNEt₂), >97%) was purchased from TCI America. Europium(III) chloride hexahydrate (EuCl₃·6H₂O, 99.9%) was purchased from Strem Chemicals. Sodium and potassium metal were purchased from AlfaAesar. Acetone (Fisher, ACS) was dried by reflux over anhydrous CaSO₄ and distilled before use. Hexanes (Fisher, ACS) were dried over sodium benzophenone and distilled before use. 2-Propanol and acetonitrile were purchased from Fisher.

Synthesis of Sodium Anthracenide. Excess sodium metal was spread in a scintillation vial to make a mirror. Anthracene (0.1 mmol)

was then added followed by 5 mL of THF. The mixture was stirred overnight to form a 0.02 M sodium anthracenide (Na[ANT]) solution. Sodium naphthalenide (0.02 M, Na[NAP]) and potassium anthracenide (0.02 M, K[ANT]) were made analogously.

Preparation of Na(Hg). Na(Hg) (0.5%) was prepared by dissolving Na metal (0.0388 g) in Hg metal (5 mL). The sodium metal was added slowly because the reaction is highly exothermic.

Diethylammonium Europium Tetrakis-Diethyldithiocarbamate (NH₂Et₂)[Eu(S₂CNEt₂)₄] (1). (NH₂Et₂)[Eu(S₂CNEt₂)₄] was prepared by adapting literature procedures. Briefly, (NH₂Et₂)-(S₂CNEt₂) (2.38 g) was added to an Erlenmeyer flask containing 70 mL of anhydrous ethanol under ambient conditions. In a separate scintillation vial, a stoichiometric amount of EuCl₃·6H₂O (0.98 g) was added to 15 mL of anhydrous ethanol. The two solutions were stirred to yield homogenous solutions. The europium solution was slowly added to the Erlenmeyer flask to form the red-orange crystals of (NH₂Et₂)[Eu(S₂CNEt₂)₄]. The mixture was stirred for 20 min to allow complete precipitation of 1, which was collected by filtration and washed with cold anhydrous ethanol several times. 1 was stored in a desiccator and used within 2 weeks of synthesis.

Synthesis of Colloidal EuS Nanocrystals. In a typical synthesis, OLA (2.43 mL) was added to a 50 mL three-necked, round-bottom flask fitted with a reflux condenser and a thermocouple for temperature control and degassed under vacuum for 30 min at 120 °C. TOP (2.27 mL) was injected into the flask, and the mixture was degassed for an additional 15 min. The solvent mixture was then heated to a temperature of 280 °C under nitrogen. In a separate scintillation vial, 1 (0.11 g) was added to OLA (1.2 mL). This mixture was stirred to produce a clear red-orange solution. The solution of 1 was injected into the reaction flask at 280 °C and maintained at this temperature for 1 h under constant stirring. The mixture was cooled to room temperature and transferred to a nitrogen-filled glovebox for further purification. The NCs were washed four times by precipitation with acetone followed by centrifugation and suspension in hexanes. The worked-up NCs were stored in the glovebox suspended in ~5 mL of hexanes, which gave a purple-colored colloidal solution.

Reduction Titrations. EuS NCs of a known concentration were suspended in a solution of THF and loaded into an air-free cuvette. For reductions using Na[ANT], K[ANT], Na[NAP], and CoCp₂*, a known amount of reductant solution was titrated in to reduce the NCs. The progress of the titration was monitored by collecting an absorption spectrum following each addition of reductant. The reduction was considered complete when features corresponding to the reductant appeared in the absorption spectrum. For reduction using Na(Hg), an amount of Na(Hg) corresponding to 600 equivalents of Na per Eu was added to a solution of EuS NCs in THF in an air-free cuvette with a Teflon stir bar. The solution was allowed to mix for several days and monitored by UV-vis-NIR spectroscopy. For reduction using Na metal, a freshly cut piece of Na metal was added to a solution of EuS NCs in THF in an air-free cuvette. The progress of the reduction reaction was monitored by UV-vis-NIR spectroscopy over a 2-week period.

EPR Measurements. Continuous-wave electron paramagnetic resonance (EPR) measurements were performed using a Bruker EMX spectrometer operated at X-band frequencies. The sample and probe were mounted inside an Oxford Instruments ESR900 continuous flow cryostat. The temperature was controlled and monitored with an Oxford Instruments ITC5035 temperature controller and a Cernox Resistor CX-1050-AA-1.4 L temperature sensor (LakeShore). Anhydrous 2-MeTHF was used as the solvent because it forms a high-quality glass. For EPR measurements of reduced EuS NCs, the reductant (0.02 M Na[ANT] dissolved in 2-MeTHF) was titrated into a solution of NCs in 2-MeTHF. The progress of the reduction was monitored by absorption spectroscopy. Once fully reduced, 350 μ L of the sample was transferred to an EPR tube for measurement. For EPR measurements of the native EuS NCs, 350 μ L of NC solution in 2-MeTHF at the same concentration as in the reduced sample was loaded into an EPR tube. For all EPR measurements, samples were kept under an N2 atmosphere.

XPS Measurements. All XPS spectra were recorded on a Surface Science Instruments S-Probe photoelectron spectrometer. This instrument has a monochromatized Al K α X-ray source that was operated at 20 mA and 10 kV and a low-energy electron flood gun for charge neutralization. Samples were drop-cast from solution onto silicon substrates and prepared under a nitrogen atmosphere. The Xray analysis area was $\sim 800 \ \mu m$ across. Pressure in the analytical chamber during spectral acquisition was $<5 \times 10^{-9}$ torr. Pass energy for survey and detailed spectra was 150 eV. Data point spacing was 1.0 eV/step for survey spectra and 0.4 eV/step for detailed spectra. For high-resolution spectra, pass energy was 50 eV and data point spacing was 0.065 eV/step. The take-off angle was 0°. Service Physics Hawk v7 data analysis software was used to calculate the elemental compositions from peak areas and to fit the peaks of the highresolution spectra. An inelastic scattering (Shirley) background was used in the analysis.

General Characterization. Unless otherwise noted, UV-vis-NIR absorption spectra were collected using a Varian Cary 5000 or an Agilent Cary 5000 spectrophotometer on THF solutions of NCs. NIR-IR measurements were performed using a Nicolet 8700 FTIR instrument. Samples were prepared for powder X-ray diffraction (XRD) by depositing NCs from solution onto a silicon substrate, and data were collected using a Bruker D8 Discover diffractometer. TEM samples were prepared by drop casting suspensions of NCs onto 400 mesh carbon-coated copper grids from TED Pella, Inc. and dried under an inert atmosphere. TEM images were obtained using a FEI TECNAI G2 F20 microscope operated at 200 kV. Size distributions were determined by analysis of >300 individual NCs. Elemental compositions were determined from nitric-acid-digested NC samples using inductively coupled plasma-atomic emission spectroscopy (ICP-AES) with a PerkinElmer 8300 spectrometer. Photoluminescence measurements were performed on drop-coated films of NCs sandwiched between quartz disks and mounted in a closed-cycle helium cryostat. A 405 nm diode laser was used for excitation, and the emission was detected using a liquid-nitrogen-cooled CCD mounted on a monochromator.

■ RESULTS AND DISCUSSION

The synthesis of colloidal EuS NCs was adapted from previous reports ¹⁹ and relies upon the high-temperature decomposition of an europium(III) dithiocarbamate precursor (see Methods). The in situ reduction of the Eu³⁺ precursor during synthesis is believed to be facilitated by the ligand and the oleylamine used as a solvent. Incomplete reduction is likely the source of some of the Eu³⁺ found in the final NCs (vide infra). To minimize any further oxidation or hydrolysis over the course of our experiments, the NCs were prepared, purified, and handled under rigorously air-free conditions unless otherwise noted.

Figure 1 summarizes the general characterization of representative as-synthesized EuS NCs. The absorption spectrum plotted in Figure 1a shows a broad band centered at 500 nm. This band corresponds to the $f-d(t_{2g})$ transition of Eu²⁺ and is considered the band gap of the material. Figure 1b shows powder X-ray diffraction data collected for the same EuS NCs. These data index well to the expected pattern for EuS (PDF# 01-071-4399) and reveal no additional crystalline phases. Figure 1c,d shows a TEM image of the sample and the associated size histogram. These data show that the NCs are approximately spherical in shape with an average diameter of 5.4 ± 1.1 nm. At this size, the particles are larger than the reported Bohr radius of ~1.8 nm and do not display quantum confinement effects. Coverall, these NCs are thus similar to those described previously.

Figure 2 plots X-ray photoelectron spectroscopy (XPS) data collected for the as-prepared EuS NCs deposited onto a silicon substrate. The survey scan in Figure 2a shows a large C 1s

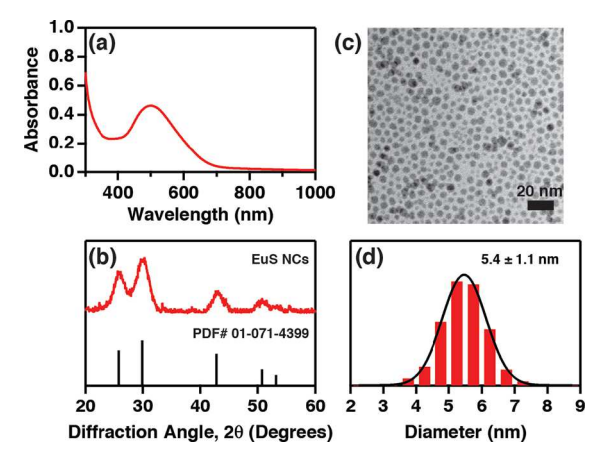


Figure 1. Characterization of colloidal EuS nanocrystals. (a) Absorption spectra collected at room temperature. The band centered at 500 nm corresponds to the $f-d(t_{2g})$ transition of Eu²⁺. (b) Powder X-ray diffraction data collected for EuS NCs drop-cast on a silicon substrate (red) and corresponding literature pattern for cubic EuS (black, PDF# 01-071-4399). The NC data match the expected peak pattern. (c) TEM image of EuS NCs, with the scale bar representing 20 nm. (d) Size distribution of NCs shown in (c) determined by measuring >300 nanocrystals, and Gaussian fit, yielding a mean diameter of 5.4 \pm 1.1 nm.

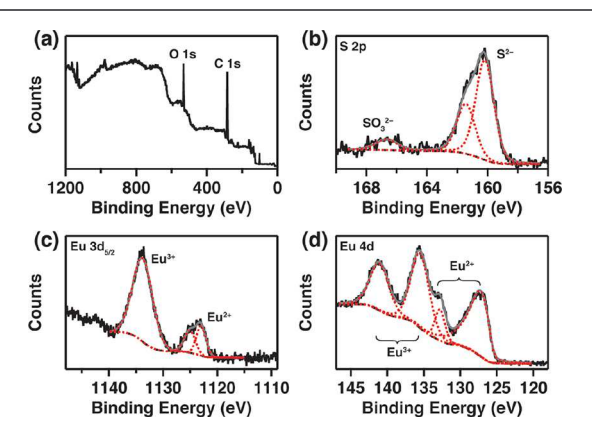


Figure 2. X-ray photoelectron spectroscopy (XPS) of EuS nanocrystals deposited on a silicon substrate. (a) Survey scan of EuS NCs. The C 1 s peak was used for energy referencing. (b) High-resolution spectra of the S 2p region. (c,d) High-resolution spectra in the Eu $3d_{5/2}$ and 4d regions, respectively. The peaks are deconvolved by simultaneously fitting an inelastic background (black dash). The convolved fit is plotted in gray.

signal that was used for energy referencing. A large O 1s signal is also observed, but because of the substrate it cannot be determined whether this signal arises in part from the NC capping ligands or from the NCs themselves. Figure 2b plots high-resolution XPS data in the S 2p region. The majority of the signal (94%) is from S²⁻ associated with the NCs. There is a small (6%) signal at 166.6 eV that is assigned to residual SO₃²⁻, most likely from oxidation of the diethyldithiocarbamate ligands used during synthesis. Figure 2c plots a highresolution scan of the Eu $3d_{5/2}$ region. Two bands are observed in this region, a lower-energy band that is fit to two Gaussian functions centered at 1122.9 and 1125.0 eV and assigned to Eu²⁺ and a higher-energy band centered at 1133.7 eV that is best fit by one Voigt function, corresponding to Eu³⁺. Both assignments are consistent with the literature.²⁷ The Eu²⁺ intensity only accounts for 24% of the total Eu $3d_{5/2}$ signal.

Figure 2d plots the spectrum in the Eu 4d region, showing three major peaks and a clear shoulder. This region is more complicated than the $3d_{5/2}$ region, and this intensity is fitted using four Voigt functions taking into account asymmetry. The two lower-energy peaks from the 4d region (127.2 and 132.7 eV) are assigned to Eu²⁺ and account for 44% of the signal, i.e., a fraction greater than that found for the Eu $3d_{5/2}$. These peaks are asymmetric because of splittings caused by the neighboring 4f electrons. The two higher-energy peaks (135.5 and 141.0 eV) are assigned to Eu³⁺ and account for 56% of the total Eu 4d signal. The extensive NC oxidation observed here is similar to what has been reported for other EuS NCs, as determined by X-ray magnetic circular dichroism and Eu-151 Mössbauer spectroscopies.

The discrepancy in the relative Eu2+ content between the $3d_{5/2}$ and 4d spectral regions results from the difference in inelastic mean-free paths (IMFPs) of electrons in these two energy regions. The $3d_{5/2}$ electrons, with their lower kinetic energy, have an IMFP that is approximately half that of the 4d electrons. This difference causes measurements in the $3d_{5/2}$ region to be more sensitive to the NC surfaces than measurements in the 4d region, especially after attenuation through the surrounding organics. In general, XPS is a surfacesensitive technique, and even the lower-energy 4d spectra selectively probe the NC surfaces. Nonetheless, taken together, these measurements indicate that these NCs have highly oxidized surfaces (>50% Eu³⁺), with the degree of oxidation decreasing closer to the NC core. These results alone cannot fully differentiate between a gradient mixture of Eu³⁺ and Eu²⁺ within the EuS lattice or a "core/shell" structure consisting of a EuS core surrounded by, for example, an amorphous oxidized shell (e.g., Eu₂O₂S). Despite the high Eu³⁺ levels indicated by XPS, absorption spectra show now indication of Eu³⁺ at room or low temperatures; however, weak $Eu^{3+} f-f$ emission is detected in the low-temperature photoluminescence spectrum of the NCs (see the Supporting Information).

To evaluate the influence of these Eu³⁺ ions on the NC magnetism, we sought to use an external reducing agent that could modify their valency. Solutions of EuS NCs in THF were treated with various reducing agents while monitoring the absorption spectra. Moderately strong reductants²⁹ such as decamethylcobaltacene (-1.94 V vs Fc⁺/Fc) and Na(Hg) (-2.36 V vs Fc⁺/Fc in THF) had no effect on the NC spectra (see the Supporting Information). Stronger reductants such as sodium anthracenide (Na[ANT], -2.47 V vs Fc⁺/Fc) did cause significant spectral changes, however, causing growth in the characteristic EuS absorption band at ~500 nm. Figure 3a plots absorption spectra of EuS NCs collected during the course of anaerobic reduction with Na[ANT]. Each spectrum in the series corresponds to an addition of 0.1 equivalents of Na[ANT] per Eu. The sharp absorption bands between 300-400 nm that appear after the first addition of Na[ANT] come from the redox product, anthracene, and the feature at \sim 740 nm that appears in the absorption spectrum after the final addition of Na[ANT] comes from the [ANT] - radical (anthracenide). Combined with the EuS NC absorption at ~500 nm, these distinct spectral features are useful for monitoring the reaction progress.

The spectral changes in Figure 3a are summarized in Figure 3b. The EuS $f-d(t_{2g})$ absorption at ~500 nm increases until ~0.4 equivalents of Na[ANT] has been added, in parallel with growth of anthracene absorption. Because Eu³⁺ is effectively optically silent at these concentrations, these data are

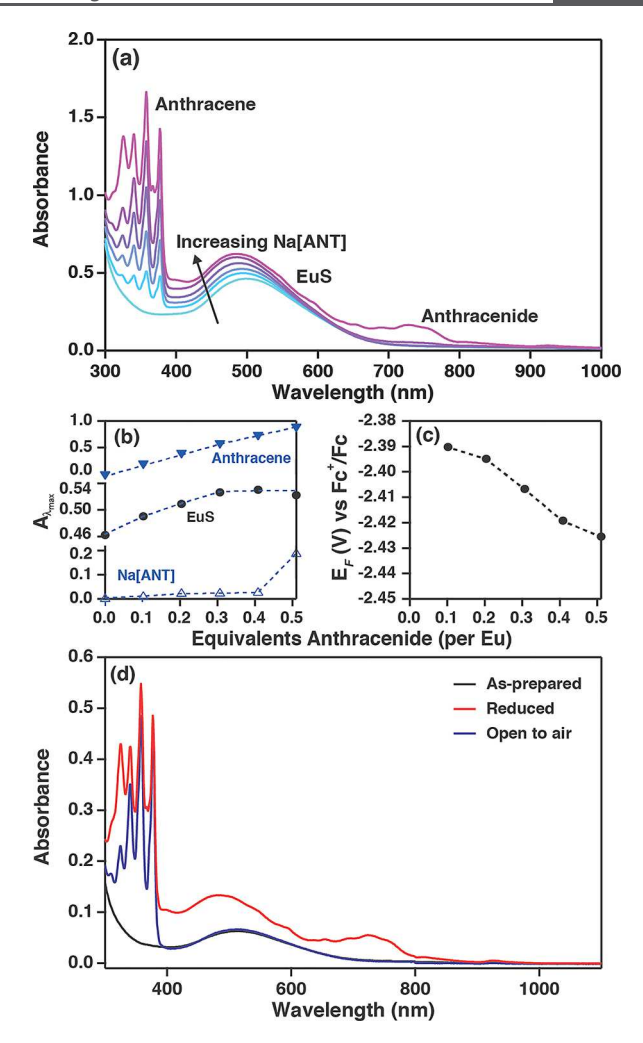


Figure 3. Chemical reduction of EuS nanocrystals using sodium anthracenide (Na[ANT]). (a) Absorption spectra of EuS NCs with different amounts of the reductant Na[ANT] added. The peaks corresponding to anthracene, EuS $f-d(t_{2g})$, and anthracenide are labeled. (b) Absorbance values of the EuS $f-d(t_{2g})$ band (~500 nm), the anthracene band (377 nm), and the Na[ANT] band (727 nm) from panel (a), plotted vs equivalents of anthracenide. (c) Fermi level of the reaction mixture from (a), determined using eq 1. The Fermi level becomes more negative as Na[ANT] is added. (d) Absorption spectra of the as-prepared EuS NCs (black), the same nanocrystals when maximally reduced (red, ~0.5 equivalents Na[ANT]), and the same nanocrystals after subsequent reoxidization by exposure to air (blue). After air oxidation, the as-prepared EuS nanocrystal absorption spectrum is recovered quantitatively, with the other spectral changes attributable to oxidation of anthacenide to anthracene.

consistent with reduction of $\mathrm{Eu^{3^+}}$ to $\mathrm{Eu^{2^+}}$ by anthracenide, forming anthracene as the reaction byproduct. Beyond ~ 0.4 equivalents, the $\mathrm{EuS}\ f-d(t_{2\mathrm{g}})$ absorption plateaus, and at 0.5 equivalents, absorption from anthracenide appears. Observation of this anthracenide absorption suggests that the reaction's equivalence point has been reached. The amount of reductant required to reach the equivalence point is thus ~ 0.5 equivalents per Eu ion, a value consistent with the observation by XPS (Figure 2) that $\sim 50\%$ of the Eu is $\mathrm{Eu^{3^+}}$. For comparison, the $f-d(t_{2\mathrm{g}})$ absorption increases by $\sim 44\%$ over the course of the same reduction reaction (Figure 3).

The $f-d(t_{2g})$ band also blue-shifts slightly (\sim 50 meV total) with added Na[ANT]. This shift contrasts with the red-shifts

observed when CB electrons are introduced into these magnetic semiconductors in bulk. 10,11 The NCs show no new intra-band absorption in the mid-IR after reduction (see the Supporting Information), confirming the absence of delocalized CB electrons. Instead, the $f-d(t_{2g})$ blue-shift is interpreted as reflecting a different coordination environment around some or all of the newly formed $\mathrm{Eu^{2+}}$ ions relative to lattice $\mathrm{Eu^{2+}}$ in EuS. For example, these newly reduced $\mathrm{Eu^{2+}}$ ions could be exposed to surface-capping ligands at the NC surfaces or could reside in an oxysulfide shell, resulting in a slightly smaller $d(t_{2g})$ ligand-field splitting and hence causing the observed blue-shift of the $f-d(t_{2g})$ transition.

As an equilibrium outer-sphere redox reaction, the Fermi level $(E_{\rm F})$ of the solution in which the NCs are reduced can be determined from the Nernst equation (eq 1).30 Here, the concentration of anthracene is measured spectroscopically using the known extinction coefficients of the bands between 300-400 nm (see the Supporting Information). The standard reduction potential of anthracene is taken as -2.47 V vs Fc^+/Fc in THF.²⁹ Figure 3c plots E_F measured in this way vs the equivalents of added anthracenide. As Na[ANT] is added, the Fermi level becomes increasingly negative, ultimately reaching ca. -2.43 V vs Fc⁺/Fc at the equivalence point. There is no discernible occupation of the EuS CB, meaning the NC band-edge potential is more negative than this potential. This result is consistent with the fact that the most negative potential measured here is ~300 mV more positive than the literature CB-edge potential of bulk EuS, $-2.7 \pm 0.3 \text{ V}$ vs Fc⁺/ Fc. 31 Similar results are obtained with even stronger reductants, however, including alkali naphthalemide (-3.10 V vs Fc^+/Fc) and sodium metal (-3.04 V vs Fc^+/Fc), ²⁹ that should be sufficiently more negative than the bulk band-edge potential to inject CB electrons. The band-edge potentials of colloidal EuS NCs have not been measured previously, but those of other colloidal NCs are known to be very sensitive to surface dipoles, shifting by as much as ±500 mV for different surface chemistries in the case of CdSe NCs³²⁻³⁴ for example. The absence of CB electrons in these EuS NCs even when reacted with such strong reductants likely reflects a similar effect here.

$$\begin{split} E_{\rm F}(V) &= E_{\rm cell}(V) \\ &= E^{\circ} - 0.02568 \; \text{ln} \; \frac{[\text{Anthracenide}]_{\rm total \; added} \; - \; [\text{Anthracene}]}{[\text{Anthracene}]} \end{split} \tag{1}$$

Collectively, these data indicate that potentials more negative than ca. -2.36 V vs Fc⁺/Fc are required to reduce Eu³⁺ to Eu²⁺ in these NCs and that the EuS NC CB-edge potential is several 100 mV more negative than this Eu^{3+/2+} potential. Because of the very negative potentials involved, the reduced NCs are themselves very strong reductants. Consequently, EuS NCs reduced by these methods are not stable in air. Upon exposing a solution of reduced EuS NCs to air, the increased $f-d(t_{2g})$ absorbance is lost and the $f-d(t_{2g})$ band red-shifts back to its starting energy (Figure 3d). Other than the presence of anthracene, the resulting spectrum is essentially indistinguishable from that collected before reduction. This similarity suggests that the NC reduction is fully reversible i.e., no degradation or other irreversible transformations occur. This conclusion is supported by TEM measurements, which also show no discernible NC degradation after reduction with Na[ANT] and re-oxidation by air (Supporting Information).

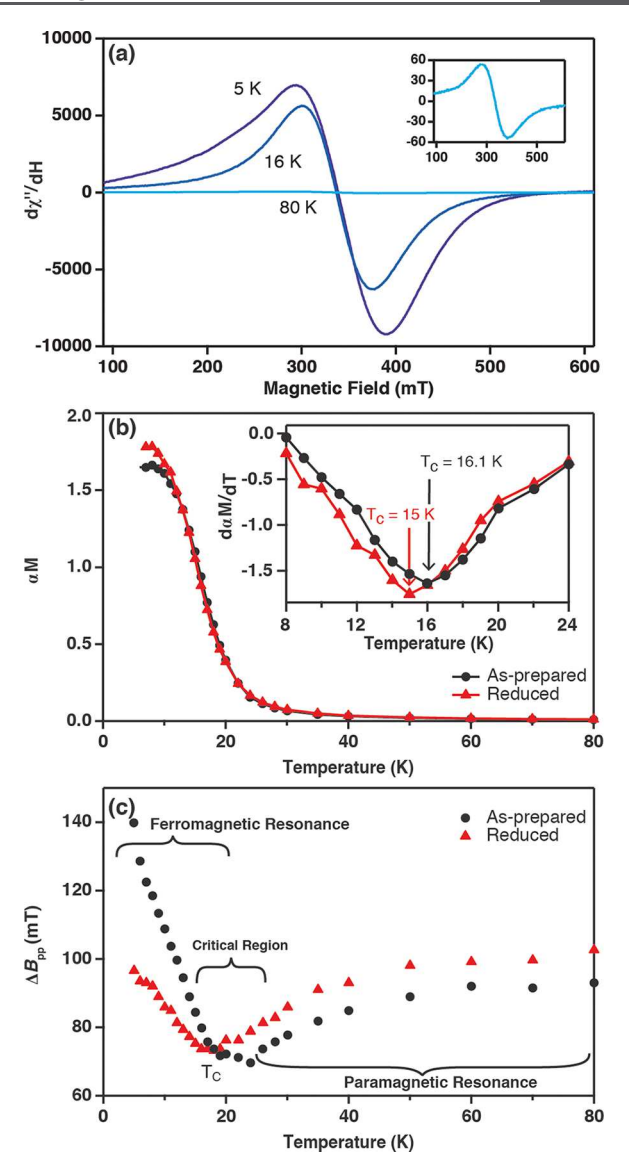


Figure 4. EPR data from the as-prepared and reduced EuS NCs. (a) Representative EPR spectra of reduced EuS NCs collected at 5, 16, and 80 K. Linewidth narrowing in the vicinity of the critical region (\sim 16 K) is apparent. The inset plots a zoom-in of the 80 K spectrum. (b) Proportional magnetization (from double-integration of the EPR spectrum) plotted vs temperature for the as-prepared (black dots) and fully reduced (red triangles) EuS NCs. Na[ANT] was used as the reductant. Curie temperatures of 16.1 and 15.0 K for the as-prepared and reduced EuS NCs, respectively, are determined from the minima in the first derivative of the magnetization data (inset). (c) Peak-to-peak linewidth ($\Delta B_{\rm pp}$) plotted vs temperature. Ferromagnetic-resonance and paramagnetic-resonance regions are indicated.

The effect of Eu reduction on the EuS NC magnetism was then probed using variable-temperature CW X-band EPR spectroscopy. As non-Kramers ions with a nonmagnetic (J=0) ground state, Eu³⁺ ions are generally EPR silent;³⁵ therefore, any EPR signal is attributable to Eu²⁺. Figure 4a plots representative EPR spectra of EuS NCs reduced with Na[ANT], measured at different temperatures. EPR spectra of the corresponding as-prepared NCs and absorption spectra indicating complete reduction are provided in the Supporting Information. The EPR intensity is greatest at the lowest temperature (5 K), and it decreases as the temperature is raised. At the highest temperature (80 K), the spectrum is very

weak. The EPR spectra in Figure 4a are plotted as $d\chi''/dH$. Integration of these spectra thus yields the EPR susceptibility, χ ", with further integration giving a value proportional to magnetization, αM . Figure 4b plots αM vs temperature for the as-prepared and reduced NCs. Both samples show a lowtemperature plateau followed by a rapid drop at higher temperature characteristic of a ferromagnetic-to-paramagnetic transition. Figure 4c plots the dependence of the EPR linewidth, $\Delta B_{\rm pp}$, on temperature for the as-prepared and reduced NCs. Upon warming from 5 K, the linewidth narrows until a similar critical temperature, beyond which it broadens again. This behavior is also characteristic of ferromagnetic-to-paramagnetic phase transitions. $^{36-41}$ The resonance of the asprepared NCs broadens significantly more than that of the reduced NCs in the ferromagnetic resonance region. We attribute this difference to the presence of Eu³⁺ in the former. Eu3+ has significant orbital angular momentum that leads to very fast spin-lattice relaxation, which broadens the ferromagnetic resonance linewidth. 42 Similarly, the Landé gfactor increases as the temperature is raised beyond the critical region (see the Supporting Information), as observed for bulk EuS. 43 By all measurements, the critical temperature of the reduced NCs is lower than that of the as-prepared (oxidized) NCs.

The Curie temperatures of these NCs are determined from the minima in the first derivative of the αM vs T data (Figure 4b, inset). From these data, $T_{\rm C}$ for the reduced EuS NCs is estimated to be 15.0 K, whereas that of the as-prepared EuS NCs is 16.1 K, corresponding to a decrease of ~7% upon NC reduction. In addition to lowering T_C , NC reduction also causes a \sim 7% increase in magnetization (αM) below $T_{\rm C}$. This result is consistent with NC reduction generating additional Eu²⁺ species that also partially align ferromagnetically with the core EuS spins. Because no delocalized CB electrons are present in either oxidized or reduced forms of these NCs, this shift in $T_{\rm C}$ cannot be attributed to the same carrier-mediated exchange mechanism as reported for bulk aliovalently doped EuS. Instead, the shift in $T_{\rm C}$ is likely attributable to the different coordination environment of the newly reduced Eu²⁺ ions indicated by the spectroscopic data discussed above, implying a weaker inter-Eu exchange coupling for these Eu²⁺ ions than within the core EuS lattice. The mechanism by which $T_{\rm C}$ depends on the presence of trivalent impurity ions in these NCs is thus fundamentally distinct from that in bulk.

CONCLUSIONS

EuS NCs prepared by literature methods were demonstrated to contain high levels of Eu³⁺ despite rigorously anaerobic NC synthesis and handling. These Eu3+ ions could be reduced to Eu²⁺ by reacting the NCs with strong chemical reducing agents. This reduction manifests itself spectroscopically as a blue-shift of the Eu²⁺ f- $d(t_{2g})$ transition and an increase in its absorbance, suggesting that the redox-active Eu ions are located predominantly at the NC surfaces and have a slightly different coordination environment. In bulk, doping EuS with trivalent lanthanides (e.g., Gd^{3+}) can increase T_C by generating excess CB-like electrons (n doping). In contrast, the data here suggest that the Eu³⁺ impurities in the as-synthesized EuS NCs do not introduce excess CB-like electrons and therefore do not have the same effect. Rather, reduction from Eu³⁺ to Eu²⁺ reduces T_C by ~7%. The experimental shift in T_C upon NC reduction is attributed to differences in Eu²⁺ coordination that cause the newly reduced Eu2+ to have weaker inter-Eu

magnetic exchange coupling, an interpretation supported by the shift in $\mathrm{Eu^{2+}} f - d(t_{2g})$ transition energies between original and newly reduced $\mathrm{Eu^{2+}}$ ions. The trivalent $\mathrm{Eu^{3+}}$ dopants also have a lower magnetic moment than Eu²⁺ ions, and reduction from Eu³⁺ to Eu²⁺ thus increases the NC magnetic moment below $T_{\rm C}$. Notably, the data show no evidence of CB-like electrons in these EuS NCs, either from the abundant Eu³⁺ impurities found in the as-prepared NCs or after exposure of these NCs to strong chemical reductants. The very negative CB-edge potentials encountered during these redox-titration measurements highlight the challenge of stabilizing CB-like electrons in colloidal EuS NCs. In contrast with aliovalent doping of bulk EuS crystals, the excess positive charges of aliovalent impurities in colloidal EuS NCs appear to be locally compensated at the NC surfaces, diminishing the effectiveness of these ions (or, by inference, also other trivalent impurities) as electronic dopants compared to bulk. Despite these differences, the results here demonstrate successful chemical reduction of colloidal EuS NCs, revealing that the NCs are stable even to very strong reductants, that this reduction is fully reversible, and that it indeed allows postsynthetic manipulation of the magnetism of the EuS NCs, albeit by a different microscopic mechanism compared to that found in bulk EuS. These results shed new light on the fundamental physicochemical properties of colloidal ferromagnetic EuS NCs and demonstrate charge-tunable magnetism in such materials for the first time.

ASSOCIATED CONTENT

s Supporting Information

The Supporting Information is available free of charge at https://pubs.acs.org/doi/10.1021/acs.chemmater.0c03020.

Additional data including low-temperature absorption and photoluminescence spectra, TEM characterization, spectra summarizing the effects of different reducing agents, reduction and reversibility data, and EPR data (PDF)

AUTHOR INFORMATION

Corresponding Authors

Sarah L. Stoll — Department of Chemistry, Georgetown University, Washington, D.C. 20057, United States; orcid.org/0000-0001-7184-8672; Email: gamelin@chem.washington.edu

Daniel R. Gamelin — Department of Chemistry, University of Washington, Seattle, Washington 98195-1700, United States; orcid.org/0000-0003-2888-9916; Email: sls55@georgetown.edu

Authors

Michael C. De Siena — Department of Chemistry, University of Washington, Seattle, Washington 98195-1700, United States; orcid.org/0000-0003-0379-5577

Alexander G. Rachkov — Department of Chemistry, University of Washington, Seattle, Washington 98195-1700, United States Rachel Fainblat — Department of Chemistry, University of Washington, Seattle, Washington 98195-1700, United States; orcid.org/0000-0002-9488-2563

Derak James — Department of Chemistry, Georgetown University, Washington, D.C. 20057, United States

Sidney E. Creutz — Department of Chemistry, University of Washington, Seattle, Washington 98195-1700, United States; orcid.org/0000-0003-4440-5336

Complete contact information is available at: https://pubs.acs.org/10.1021/acs.chemmater.0c03020

Notes

The authors declare no competing financial interest.

ACKNOWLEDGMENTS

The nanocrystal redox titrations and Fermi level analysis were supported by the U.S. National Science Foundation through project CHE-1904436 (to D.R.G.). The nanocrystal synthesis and spectroscopic measurements were partially supported by the U.S. National Science Foundation through the UW Molecular Engineering Materials Center (MEM-C), a Materials Research Science and Engineering Center (DMR-1719797). The contributions of the Stoll group were supported by the U. S. National Science Foundation (both CHE-1607905 and CHE-1904616). R.F. was also supported by the P.R.I.M.E. program from the German Academic Exchange Service (DAAD) with funds from the German Federal Ministry of Education and Research (BMBF) and the People Programme (Marie Curie Actions) of the European Union's Seventh Framework Programme (FP7/2007-2013). This research was additionally partially supported by an appointment to the Intelligence Community Postdoctoral Research Fellowship Program at UW (S.E.C.), administered by Oak Ridge Institute for Science and Education through an interagency agreement between the U.S. Department of Energy and the Office of the Director of National Intelligence. Part of this work was conducted at the Molecular Analysis Facility, a National Nanotechnology Coordinated Infrastructure site at the University of Washington that is supported in part by the National Science Foundation (grant ECC-1542101), the University of Washington, the Molecular Engineering & Sciences Institute, the Clean Energy Institute, and the National Institutes of Health. Mr. Gerry Hammer is acknowledged for assistance with the XPS measurements. Mr. Donald Mannikko and Dr. Ellen Hayes are acknowledged for assistance with the variable-temperature EPR measurements.

■ REFERENCES

- (1) Mauger, A.; Godart, C. The magnetic, optical, and transport properties of representatives of a class of magnetic semiconductors: The europium chalcogenides. *Phys. Rep.* **1986**, *141*, 51–176.
- (2) Moodera, J. S.; Hao, X.; Gibson, G. A.; Meservey, R. Electron-Spin Polarization in Tunnel Junctions in Zero Applied Field with Ferromagnetic EuS Barriers. *Phys. Rev. Lett.* **1988**, *61*, 637–640.
- (3) Moodera, J. S.; Santos, T. S.; Nagahama, T. The phenomena of spin-filter tunnelling. *J. Phys. Condens. Matter* **2007**, *19*, 165202.
- (4) De Simoni, G.; Strambini, E.; Moodera, J. S.; Bergeret, F. S.; Giazotto, F. Toward the Absolute Spin-Valve Effect in Superconducting Tunnel Junctions. *Nano Lett.* **2018**, *18*, 6369–6374.
- (5) Kar, S.; Boncher, W. L.; Olszewski, D.; Dollahon, N.; Ash, R.; Stoll, S. L. Gadolinium Doped Europium Sulfide. *J. Am. Chem. Soc.* **2010**, *132*, 13960–13962.
- (6) Selinsky, R. S.; Han, J. H.; Morales Pérez, E. A.; Guzei, I. A.; Jin, S. Synthesis and Magnetic Properties of Gd Doped EuS Nanocrystals with Enhanced Curie Temperatures. *J. Am. Chem. Soc.* **2010**, *132*, 15997–16005.
- (7) McGuire, T. R.; Holtzberg, F. Magnetic Ordering of $Eu_{(1-x)}Gd_xS$. AIP Conf. Proc. 1972, 5, 855-859.

- (8) Mairoser, T.; Schmehl, A.; Melville, A.; Heeg, T.; Canella, L.; Böni, P.; Zander, W.; Schubert, J.; Shai, D. E.; Monkman, E. J.; Shen, K. M.; Schlom, D. G.; Mannhart, J. Is There an Intrinsic Limit to the Charge-Carrier-Induced Increase of the Curie Temperature of EuO? *Phys. Rev. Lett.* **2010**, *105*, 257206.
- (9) von Molnár, S.; Kasuya, T. Evidence of Band Conduction and Critical Scattering in Dilute Eu-Chalcogenide Alloys. *Phys. Rev. Lett.* **1968**, *21*, 1757–1761.
- (10) Schoenes, J.; Wachter, P. Exchange optics in Gd-doped EuO. *Phys. Rev. B* **1974**, *9*, 3097–3105.
- (11) Bebenin, N. G. On magnetic red shift of absorption edge in EuO. Solid State Commun. 1985, 55, 823-825.
- (12) Gambino, R. J.; Fumagalli, P.; Ruf, R. R.; McGuire, T. R.; Bojarczuk, N. Magneto-optic spectra of EuS-Gd and EuS-Tb films. *IEEE Trans. Magn.* **1992**, *28*, 2973–2975.
- (13) Schimpf, A. M.; Knowles, K. E.; Carroll, G. M.; Gamelin, D. R. Electronic Doping and Redox-Potential Tuning in Colloidal Semi-conductor Nanocrystals. *Acc. Chem. Res.* **2015**, *48*, 1929–1937.
- (14) Mairoser, T.; Loder, F.; Melville, A.; Schlom, D. G.; Schmehl, A. Influence of chemical doping on the magnetic properties of EuO. *Phys. Rev. B* **2013**, *87*, No. 014416.
- (15) Reisner, A.; Kasinathan, D.; Wirth, S.; Tjeng, L. H.; Altendorf, S. G. Valence state of Sm in single-crystalline EuO thin films. *EPL* **2017**, *117*, 47001.
- (16) Hedman, L.; Rao, K. V.; Yeshurun, Y. Magnetic properties of Eu substituted SmS. J. Appl. Phys. 1981, 52, 2155-2157.
- (17) Mirkovic, T.; Hines, M. A.; Nair, P. S.; Scholes, G. D. Single-Source Precursor Route for the Synthesis of EuS Nanocrystals. *Chem. Mater.* **2005**, 17, 3451–3456.
- (18) Zhao, F.; Sun, H.-L.; Su, G.; Gao, S. Synthesis and Size-Dependent Magnetic Properties of Monodisperse EuS Nanocrystals. *Small* **2006**, 2, 244–248.
- (19) Regulacio, M. D.; Kar, S.; Zuniga, E.; Wang, G.; Dollahon, N. R.; Yee, G. T.; Stoll, S. L. Size-Dependent Magnetism of EuS Nanoparticles. *Chem. Mater.* **2008**, *20*, 3368–3376.
- (20) Selinsky, R. S.; Keavney, D. J.; Bierman, M. J.; Jin, S. Element-specific magnetometry of EuS nanocrystals. *Appl. Phys. Lett.* **2009**, *95*, 202501.
- (21) Hasegawa, Y.; Kumagai, M.; Kawashima, A.; Nakanishi, T.; Fujita, K.; Tanaka, K.; Fushimi, K. First Synthesis of EuS Nanoparticle Thin Film with a Wide Energy Gap and Giant Magneto-Optical Efficiency on a Glass Electrode. *J. Phys. Chem. C* **2012**, *116*, 19590–19596
- (22) Johnson, C. E.; Costa, L.; Johnson, J. A.; Brown, D. E.; Somarajan, S.; He, W.; Dickerson, J. H. Mössbauer spectra and superparamagnetism of europium sulfide nanoparticles. *J. Phys. D: Appl. Phys.* **2014**, *47*, No. 075001.
- (23) Boncher, W.; Dalafu, H.; Rosa, N.; Stoll, S. Europium chalcogenide magnetic semiconductor nanostructures. *Coord. Chem. Rev.* 2015, 289-290, 279–288.
- (24) Zhao, F.; Sun, H.-L.; Gao, S.; Su, G. Magnetic properties of EuS nanoparticles synthesized by thermal decomposition of molecular precursors. *J. Mater. Chem.* **2005**, *15*, 4209–4214.
- (25) Hasegawa, Y.; Maeda, M.; Nakanishi, T.; Doi, Y.; Hinatsu, Y.; Fujita, K.; Tanaka, K.; Koizumi, H.; Fushimi, K. Effective Optical Faraday Rotations of Semiconductor EuS Nanocrystals with Paramagnetic Transition-Metal Ions. J. Am. Chem. Soc. 2013, 135, 2659—2666.
- (26) Zhou, X.; Zhang, K. H. L.; Xiong, J.; Park, J.-H.; Dickerson, J. H.; He, W. Size- and dimensionality-dependent optical, magnetic and magneto-optical properties of binary europium-based nanocrystals: EuX (X = O, S, Se, Te). *Nanotechnology* **2016**, *27*, 192001.
- (27) Vercaemst, R.; Poelman, D.; Fiermans, L.; Van Meirhaeghe, R. L.; Laflère, W. H.; Cardon, F. A detailed XPS study of the rare earth compounds EuS and EuF₃. *J. Electron Spectrosc. Relat. Phenom.* **1995**, 74, 45–56.
- (28) Kowalczyk, S. P.; Edelstein, N.; McFeely, F. R.; Ley, L.; Shirley, D. A. X-ray photoemission spectra of the 4d levels in rare-earth metals. *Chem. Phys. Lett.* **1974**, *29*, 491–495.

- (29) Connelly, N. G.; Geiger, W. E. Chemical Redox Agents for Organometallic Chemistry. *Chem. Rev.* **1996**, *96*, 877–910.
- (30) Carroll, G. M.; Schimpf, A. M.; Tsui, E. Y.; Gamelin, D. R. Redox Potentials of Colloidal n-Type ZnO Nanocrystals: Effects of Confinement, Electron Density, and Fermi-Level Pinning by Aldehyde Hydrogenation. *J. Am. Chem. Soc.* **2015**, *137*, 11163–11169.
- (31) Eastman, D. E.; Holtzberg, F.; Methfessel, S. Photoemission Studies of the Electronic Structure of EuO, EuS, EuSe, And GdS. *Phys. Rev. Lett.* **1969**, 23, 226–229.
- (32) Brown, P. R.; Kim, D.; Lunt, R. R.; Zhao, N.; Bawendi, M. G.; Grossman, J. C.; Bulović, V. Energy Level Modification in Lead Sulfide Quantum Dot Thin Films through Ligand Exchange. *ACS Nano* 2014, *8*, 5863–5872.
- (33) Carroll, G. M.; Tsui, E. Y.; Brozek, C. K.; Gamelin, D. R. Spectroelectrochemical Measurement of Surface Electrostatic Contributions to Colloidal CdSe Nanocrystal Redox Potentials. *Chem. Mater.* **2016**, *28*, 7912–7918.
- (34) Kroupa, D. M.; Vörös, M.; Brawand, N. P.; McNichols, B. W.; Miller, E. M.; Gu, J.; Nozik, A. J.; Sellinger, A.; Galli, G.; Beard, M. C. Tuning colloidal quantum dot band edge positions through solution-phase surface chemistry modification. *Nat. Commun.* **2017**, *8*, 15257.
- (35) Jewett, J. W.; Wigen, P. E. EPR of Tb³⁺, Pr³⁺, Gd³⁺, and Eu³⁺ ions in single crystal La₂O₂S. *J. Chem. Phys.* **1974**, *61*, 2991–2995.
- (36) Huber, D. L.; Seehra, M. S. Contribution of the spin-phonon interaction to the paramagnetic resonance linewidth of CrBr₃. *J. Phys. Chem. Solids* **1975**, *36*, 723–725.
- (37) Kondal, S. C.; Seehra, M. S. Shape dependence of the EPR linewidth, resonance field and spin-spin relaxation rate of EuS near Tc. J. Phys. C Solid State Phys. 1982, 15, 2471.
- (38) Oseroff, S. B.; Torikachvili, M.; Singley, J.; Ali, S.; Cheong, S. W.; Schultz, S. Evidence for collective spin dynamics above the ordering temperature in $La_{1-x}Ca_xMnO_{3+\delta}$. *Phys. Rev. B* **1996**, 53, 6521–6525.
- (39) Causa, M. T.; Tovar, M.; Caneiro, A.; Prado, F.; Ibañez, G.; Ramos, C. A.; Butera, A.; Alascio, B.; Obradors, X.; Piñol, S.; Rivadulla, F.; Vázquez-Vázquez, C.; López-Quintela, M. A.; Rivas, J.; Tokura, Y.; Oseroff, S. B. High-temperature spin dynamics in CMR manganites: ESR and magnetization. *Phys. Rev. B* 1998, *58*, 3233–3239
- (40) Huber, D. L.; Alejandro, G.; Caneiro, A.; Causa, M. T.; Prado, F.; Tovar, M.; Oseroff, S. B. EPR linewidths in $La_{1-x}Ca_xMnO_3$: $0 \le x \le 1$. Phys. Rev. B 1999, 60, 12155–12161.
- (41) Niebieskikwiat, D.; Sánchez, R. D.; Caneiro, A.; Morales, L.; Vásquez-Mansilla, M.; Rivadulla, F.; Hueso, L. E. High-temperature properties of the Sr₂FeMoO₆ double perovskite: Electrical resistivity, magnetic susceptibility, and ESR. *Phys. Rev. B* **2000**, *62*, 3340–3345.
- (42) Turov, E. A. Line width of ferromagnetic resonance absorption. In *Ferromagnetic Resonance*; Vonsovskii, S. V., Ed.; Pergamon: London, 1966; pp. 184–230.
- (43) von Molnar, S.; Lawson, A. W. Ferromagnetic and Paramagnetic Resonance in EuS. Phys. Rev. 1965, 139, A1598-A1602.